

Observation of the Pinch-Off Effect during Electrostatically Gating the Metal-Insulator Transition

Takeaki Yajima* and Akira Toriumi

Electrostatically controlling material phases has been a long-standing challenge. While it is partially achieved by electrostatic gating with ionic liquid, it often involves unintended chemical reactions. In this sense, it has recently attracted tremendous attention that a solid-state electrostatic gating is successfully applied to insulator-metal transition by using ultrahigh-permittivity gate dielectrics. However, the detailed characteristics of this new class of device are totally unknown. Here, systematic studies are performed on the three-terminal device using VO₂ insulator-metal transition and TiO₂ gate dielectrics, and for the first time the pinch-off effect in phase transition devices is observed, a clear sign of electrostatic gating. Furthermore, the increase in the drain voltage has a “catalytic effect” of drastically sharpening the gate-induced transition, demonstrating a 0.1 V gate control. The characteristics are simulated by a quasi-equilibrium model, providing the firm ground for electrical control of material phases with high speed and high resolution.

1. Introduction

Transition metal oxides exhibit a wide variety of electronic and crystalline phases due to the interaction between electronic and lattice degrees of freedom.^[1] Electrically controlling these phases with a gate voltage has been a long-standing challenge in materials science.^[2] Such an electrostatic gating technique will enable high-precision and high-speed control of material phases, which is expected to lead to scientific and engineering findings via clarification of the dynamics of the transition^[3,4] and discovery of hidden nonequilibrium phases.^[5] This electrostatic gating has been partially realized by three-terminal devices using ionic liquid gating.^[6–12] There, a vast amount of electric charge can be accumulated by using a large capacitance component formed at the solid–liquid interface to induce the phase transition. However, ionic liquids often induce electrochemical reactions at the solid–liquid interface simultaneously, making well-defined control difficult.^[12] Furthermore, the nature of ionic liquids makes

it difficult to control the gate with high precision and speed, which has limited the research on electrical phase control.


Although solid-state gating using gate dielectrics can avoid the above problem of ionic liquid gating, the gate dielectrics have a relatively small electrical capacitance and it was difficult to accumulate enough charge for phase control.^[13–17] Recently, however, it has been experimentally demonstrated that the metal-insulator transition of VO₂ ultrathin film can be controlled by solid-state gating using TiO₂ dielectrics with ultrahigh dielectric constant.^[18] Here, the metal-insulator transition in VO₂ is an archetypical phase transition between the insulating phase and the metallic phase, which is usually controlled by temperature,^[19] pressure,^[20] and impurity doping.^[21,22] The use of this solid-state

device will enable the study of material phase control in a level totally different from the past. However, the detailed characteristics of this new class of devices have not been investigated at all. In fact, the pinch-off effect, a well-known phenomenon of current saturation in silicon transistors,^[23] should occur when gate control is based on the electrostatic effect. However, even this most fundamental phenomenon has not been observed in this phase transition device. It is essential to clarify these fundamental properties for the advanced control of material phases using the three-terminal geometry.

Here, we performed a systematic study on three-terminal devices based on the metal-insulator transition of VO₂, and succeeded in observing the pinch-off effect for the first time in a phase transition device. Because the pinch-off effect is a phenomenon unique to electrostatic gating, it corroborates that the gate-induced phase transition in this device is due to the electrostatic effect. On the other hand, small Joule heat is generated when the drain voltage becomes large. It was clarified that the Joule heat, which is too small to influence the transition point, has a “catalytic” effect to dramatically steepen the phase transition. By utilizing this “catalytic” effect near the transition point, it was demonstrated that a gate voltage of about 0.1 V can induce the phase transition and a steep current change by more than two orders of magnitude. Furthermore, the three-terminal characteristics including both the pinch-off effect and the drain-voltage “catalytic” effect can be quantitatively reproduced by using a quasi-equilibrium model that includes the electrostatic effect of the gate voltage and the subtle thermal effect due to the drain voltage. These results provide a basis for three-terminal devices based on phase transitions, which contributes to the

T. Yajima
 Department of Electronics
 Kyushu University
 Fukuoka-shi, 819-0395, Fukuoka, Japan
 E-mail: yajima@ed.kyushu-u.ac.jp

A. Toriumi
 Department of Materials Engineering
 University of Tokyo
 Bunkyo, 113-8656, Tokyo, Japan

 The ORCID identification number(s) for the author(s) of this article can be found under <https://doi.org/10.1002/aelm.202100842>.

DOI: 10.1002/aelm.202100842

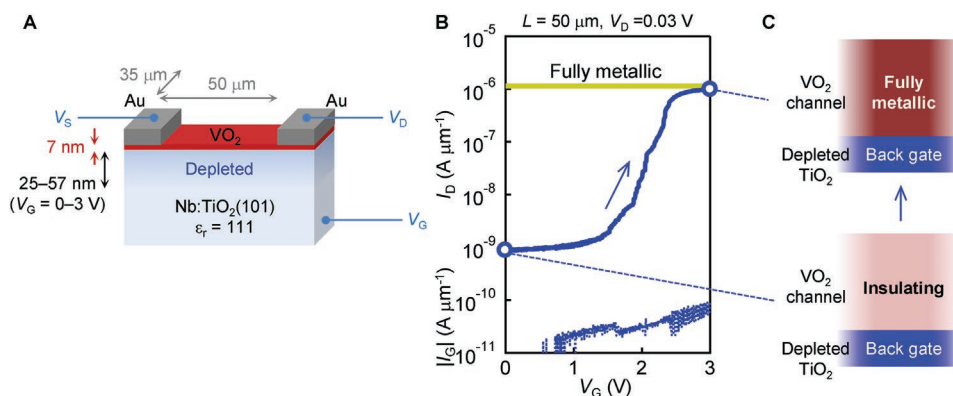


Figure 1. VO₂ channel three-terminal device. A) An illustration of the ultrathin VO₂ channel three-terminal device with the TiO₂ gate dielectrics. B) Transfer characteristics of the VO₂ channel three-terminal device at 323.5 K. The gate leakage current (I_G) is also plotted by the dotted curve. The horizontal line indicates the I_D for the fully metallic VO₂ with a resistivity of $3.7 \times 10^{-4} \Omega \text{ cm}$, which is extracted from the temperature dependence in Figure 4B. C) Illustrations of the gate-induced transition to the fully metallic VO₂ channel.

design of nonvolatile memories, low-voltage switches, neuromorphic devices, etc. In addition, it will provide a powerful tool for materials research by enabling precise or high-speed control of material phases and elucidating the transient properties.

2. Results and Discussion

2.1. VO₂-Channel Three-Terminal Device

The fabricated device consists of an epitaxial Schottky junction between the VO₂ thin film and the Nb:0.05 wt% doped TiO₂ (Nb:TiO₂) substrate, as shown in Figure 1A, which was reported previously.^[18] Here, the Nb:TiO₂ is the N-type semiconductor with a built-in potential (V_b) of 0.7 V. When the junction is reverse-biased, electrons are accumulated in the VO₂ channel (inverse Schottky gate). The depletion region in the Nb:TiO₂ substrate works as the gate dielectric with the relative permittivity of 111 and has a thickness in the range of 25–57 nm for a gate voltage in the range of 0–3 V according to the Schottky–Mott model.^[23] This large permittivity achieves an equivalent SiO₂ thickness in the range of 0.9–2 nm, and yields an accumulated electron density of the order of $1 \times 10^{14} \text{ cm}^{-2}$ that is difficult to achieve for the standard gate dielectrics, such as SiO₂ and HfO₂.

Compared with the previous report,^[18] the quality of the VO₂ thin film is improved considerably as evidenced by the more abrupt metal–insulator transition. As a result, the complete three-order change in the drain current I_D (A μm^{−1}) is induced by the gate voltage V_G (V) for the first time, as shown in Figure 1B. Because the drain voltage V_D (V) is sufficiently small (0.03 V), and the gate leakage current I_G (A μm^{−1}) is negligible, the observed gate-induced transition originates from the electrostatic effect and is not caused by Joule heating. A comprehensive discussion on this topic is listed in Supporting Information and also in ref. ^[18]. This demonstration of the complete metallic transition by solid-state electrostatic gating provides an ideal test bed for the systematic study of the three-terminal phase-transition device. The transfer curve in Figure 1B shows a gradual increase in I_D with V_G that is indicative of a typical inhomogeneous phase transition in the VO₂ channel.^[24,25]

When the V_G is small, the VO₂ channel is insulating with a sheet current density of $I_D = 8.9 \times 10^{-10} \text{ (A μm}^{-1}\text{)}$ normalized by the channel width. As the V_G crosses the transition point, the I_D increases by three orders and reaches the value of $1.0 \times 10^{-6} \text{ A μm}^{-1}$ at $V_G = 3 \text{ V}$. This I_D value coincides with the value for the fully metallic VO₂ at higher temperatures (325 K for example) as indicated by the horizontal line in Figure 1B. This coincidence indicates that the entire VO₂ channel (not only in the vicinity of the interface) becomes metallic by the application of V_G , as schematically illustrated in Figure 1C. This is also physically reasonable in terms of free energy when we consider the extra energy needed for the formation of the phase domain boundary.^[25–27]

2.2. Three-Terminal Characteristics

The transfer characteristics (I_D vs V_G) change dramatically in larger V_D cases, as shown in Figure 2A. For $V_D = 1 \text{ V}$, the gate-induced transition becomes sharp. This abrupt transition is characterized by the discontinuous jump of I_D at $V_G = 2 \text{ V}$ and by the resultant I_D value of $3.4 \times 10^{-5} \text{ A μm}^{-1}$. This I_D value indicates that the transition occurs throughout the VO₂ channel rather than at the interface or in the filamentary region. Importantly, at V_G which is just below the critical value, the I_D seems to saturate as a function of V_D and contributes to a larger discontinuous jump at the transition. The I_D saturation with V_D is more clearly observed in the output characteristics (I_D vs V_D) at $V_G = 1.8 \text{ V}$ (Figure 2B), where the I_D is almost constant as a function of V_D . This I_D saturation is known as a pinch-off effect in silicon field-effect transistors, and is a unique characteristic to electrostatic gating in three-terminal devices. Therefore, the observation of this I_D saturation corroborates the electrostatic origin underlying the basic device characteristics. The details on this pinch-off effect will be discussed later in the device simulation. The above characteristics are summarized in the V_G – V_D phase diagram in Figure 2C. While the metallic phase and the insulating phase are continually connected for the small V_D , they are separated by the discontinuous line for the large V_D .

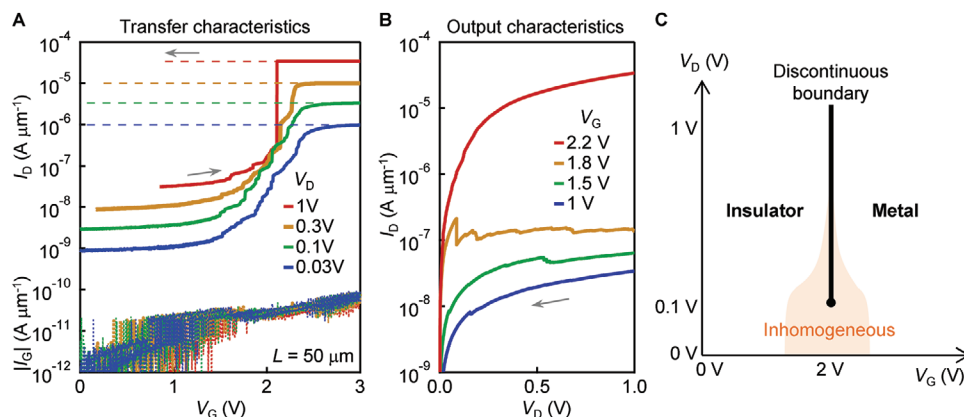


Figure 2. Three-terminal device characteristics. A) Transfer characteristics of the VO₂ channel three-terminal device at 323.5 K. V_D is set to 1, 0.3, 0.1, and 0.03 V, respectively, and I_D is plotted as a function of V_G . $|I_G|$ is also plotted simultaneously by the dotted curves. B) Output characteristics of the VO₂ channel three-terminal device. I_D is plotted as a function of V_D at four different V_G values. Measurements are performed in the direction of decreasing V_D to avoid the influence of the transition hysteresis. C) The V_G - V_D phase diagram of the VO₂ channel in the three-terminal device.

Along with the pinch-off effect, another remarkable effect is the steepening of the transition by V_D . By using this V_D effect, the transition can be induced even at a low V_G of about 0.1 V, as shown in Figure 3A,B, near the transition temperature of VO₂. Figure 3A,B shows the I_S versus V_G transfer characteristics at $V_D = 1$ V, where I_S changes almost discontinuously around $V_G = 0.1$ V. This phase transition at low V_G is only possible by using the V_D effect, since the change in I_D becomes gradual at small V_D . Here, the reason why I_S is plotted instead of I_D is that under the condition of $V_G < V_D$, the drain-to-gate junction becomes the forward biased state of the Schottky junction, and a large current flows between them and is added to I_D . This drain-to-gate current is observed in Figure 3A,B as an increase in I_G in the small V_G region. It should be noted, however, that the origin of the observed V_G -induced transition is electrostatic and not thermal, because VO₂ is insulating for

larger drain-to-gate current showing the opposite direction from the Joule heating effect.

To understand the V_D effect, it is worth noting that the V_G -induced transition for the small V_D can be regarded as a quasi-equilibrium phase transition. This is clearly observed by comparing the electrostatic gating at $V_D = 0.03$ V in Figure 4A and the temperature-induced transition in Figure 4B,C. In Figure 4B, the temperature-dependent VO₂ resistivity is plotted for various V_G . The transition temperature is negatively shifted by V_G for both heating and cooling, thus indicating that the free energy of the metallic phase is lowered by V_G with respect to the insulating phase. Specifically, the negative shift of the transition temperature is proportional to the increase in the accumulated electron density in the VO₂ channel, which is, then, proportional to $(V_G + V_b)^{1/2} - V_b^{1/2}$ (V_b : built-in potential at zero bias) (Figure S2B, Supporting Information).^[18,23] Therefore, the free energy of the VO₂ channel can be described as a function of temperature (T) and $(V_G + V_b)^{1/2} - V_b^{1/2}$. In other words, it could be expressed as a function of the “electrostatic temperature” $T_{es} = T + a\{(V_G + V_b)^{1/2} - V_b^{1/2}\}$ (K) (a : linear coefficient) to the first approximation (see Experimental Section for more details on T_{es}). Indeed, the analysis in terms of T_{es} causes all the conductivity data in Figure 4A,C to collapse, as shown in Figure 4D, wherein the conductivity in Figure 4C is calculated from the resistivity–temperature data in Figure 4B. Thus, the electrostatic gating for the small V_D can be described as a quasi-equilibrium phase transition with T_{es} in analogy to the equilibrium phase transition with T .

2.3. Device Simulation

In contrast to the purely electrostatic gating at small V_D , the nonequilibrium Joule heating may be relevant for large V_D . However, the V_D does not largely change the critical V_G for the transition, as shown in Figure 2A, thus indicating that the V_D -induced Joule heating is a secondary effect during the electrostatic gating. In the sense that it is a secondary effect, the observed V_D effect is not simply understood in the same way as the Joule heating in the two-terminal devices.^[28] To elucidate

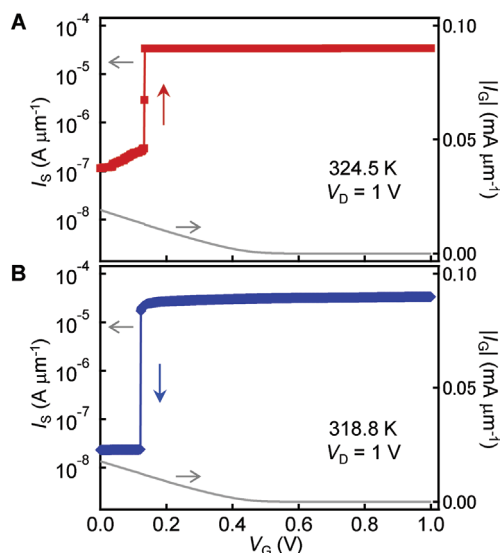


Figure 3. Low- V_G switching characteristics. I_S and I_G are measured as a function of V_G at $V_D = 1$ V. A) The insulator-to-metal transition at 324.5 K that is induced by increasing V_G . B) The metal-to-insulator transition at 318.8 K that is induced by decreasing V_G .

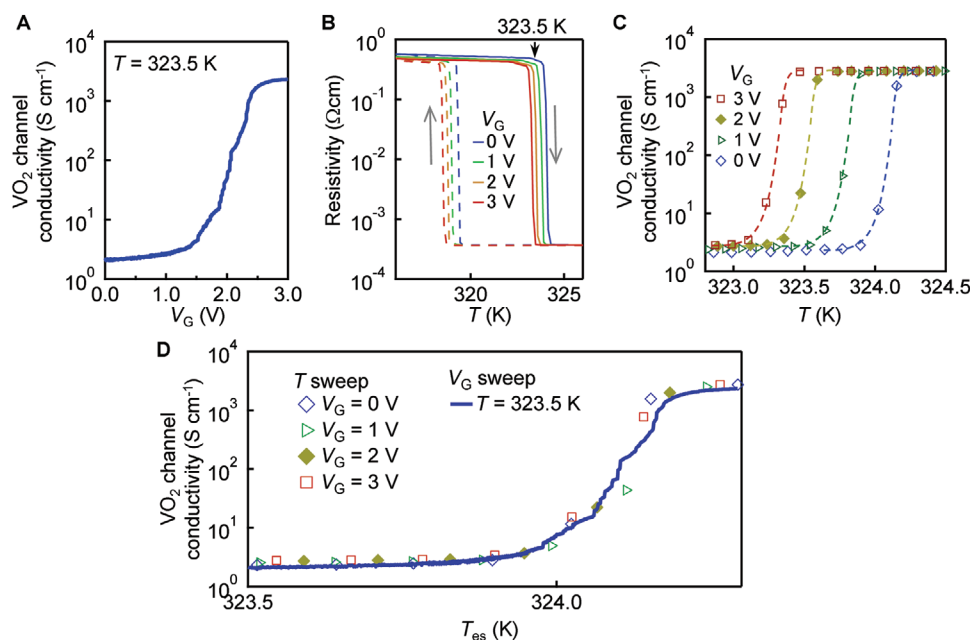


Figure 4. Quasi-equilibrium transition. A) VO₂ channel conductivity as a function of V_G at 323.5 K ($V_D = 0.03$ V). B) Temperature dependence of the VO₂ channel resistivity at four different V_G values. The V_D is small enough (0.05 V) and does not influence the transition of the VO₂ channel. The black arrow (323.5 K) indicates the measurement temperature for the three-terminal characteristics in Figure 2. C) The VO₂ channel conductivity as a function of T at $V_D = 0.05$ V for various V_G values (0–3 V). The data correspond to the heating curves in (B). The dashed curves are the guide for the eye. D) Comparison of the V_G -sweep transition at $T = 323.5$ K (from [A]) and the T -sweep transition (from [C]). T and the V_G are converted to T_{es} , and the T_{es} dependence of the VO₂-channel conductivities is plotted.

the V_D effect, the steady-state characteristics of the VO₂-channel three-terminal device are simulated in the 3D space of V_G – V_D – I_D (Figure 5A). Its 2D projection onto the V_G – V_D plane corresponds to the phase diagram of Figure 2C. In the simulation, the influences of the electrostatic gating and the Joule heating are both taken into account in the form of the local electrostatic temperature $T_{es}(x)$ (K), that yields the resistivity profile in the channel, and these two were solved self-consistently in the three-terminal device structure (see Experimental Section for details). The variable x is defined as the distance from the source. The simulated transfer characteristics in Figure 5B and the output characteristics in Figure 5C approximately reproduce the experimental data in Figure 2A,B, respectively. The local electrical potential $V_{CC}(x)$ (V) and the local sheet resistance $R_{SH}(x)$ (Ω) inside the VO₂ channel are plotted for $V_D = 1$ V in Figure 5D,E. Herein, the $V_{CC}(x)$ is defined as the channel potential with respect to the gate, and its absolute value equals the local gate voltage. In Figure 5F, the contributions from the electrostatic gating and from Joule heating are plotted separately in terms of the increase in the local electrostatic temperature $\Delta T_{es}(x)$.

For small V_G values ($V_G = 1$ V for example, the point “A” in Figure 5B), the VO₂ channel can be viewed as a normal resistor of the insulating VO₂ phase. Indeed, the $|V_{CC}(x)|$ is linearly varying with respect to x (the curve “1 V” in Figure 5D), and the $R_{SH}(x)$ value is relatively large for all the x values (the curve “1 V” in Figure 5E). When the V_G approaches 2 V (point “B” in Figure 5B), I_D is saturated at larger V_D values (the curve “2.0” in Figure 5C). Indeed, as shown by the $R_{SH}(x)$ curve for $V_G = 2$ V (Figure 5E), the metallic transition is

suppressed around the drain owing to the reduction of the local gate voltage (the curve “2 V” in Figure 5D). Thus, most of the V_D drop is in the vicinity of the drain, does not affect the electric field at the source, and has a minor influence on the I_D (see Supporting Information for details). This phenomenon is reminiscent of the pinch-off effect in the silicon field-effect transistors, wherein a similar I_D saturation was induced by the carrier depletion at the drain when the V_D increased.^[23] In other words, this I_D saturation is a unique phenomenon of electrostatic gating (Supporting Information), corroborating that the electrostatic gating is the major driving force responsible for the transition. Because of the I_D saturation, I_D maintains a relatively small value at $V_G = 2$ V (point “B” in Figure 5B) and contributes to the large discontinuous jump at the larger V_G . At $V_G = 2.09$ V (point “C” in Figure 5B), the electrostatic gating sufficiently decreases the channel resistance making the V_D -induced Joule heating non-negligible at large V_D values. Joule heating specifically occurs at the drain, as shown by the plot “2.09 V” in Figure 5F, and accelerates the metallic transition at the drain. Thus, the electrostatically induced metallic transition triggers non-negligible Joule heating at the drain, and this Joule heat is responsible for the abruptness; it weakens the I_D saturation effect and induces the discontinuous I_D jump from point “C” to point “D” in Figure 5B,C. The details of this discontinuous jump are discussed in Figure S3, Supporting Information. Above the critical gate voltage (for example $V_G = 2.1$ V, i.e., point “D” in Figure 5B), the VO₂ channel becomes completely metallic (the curve “2.1 V” in Figure 5E) and results in the linear potential profile in the channel (the curve “2.1 V” in Figure 5D). In the fully metallic state, Joule heating is too large to be plotted in Figure 5F.

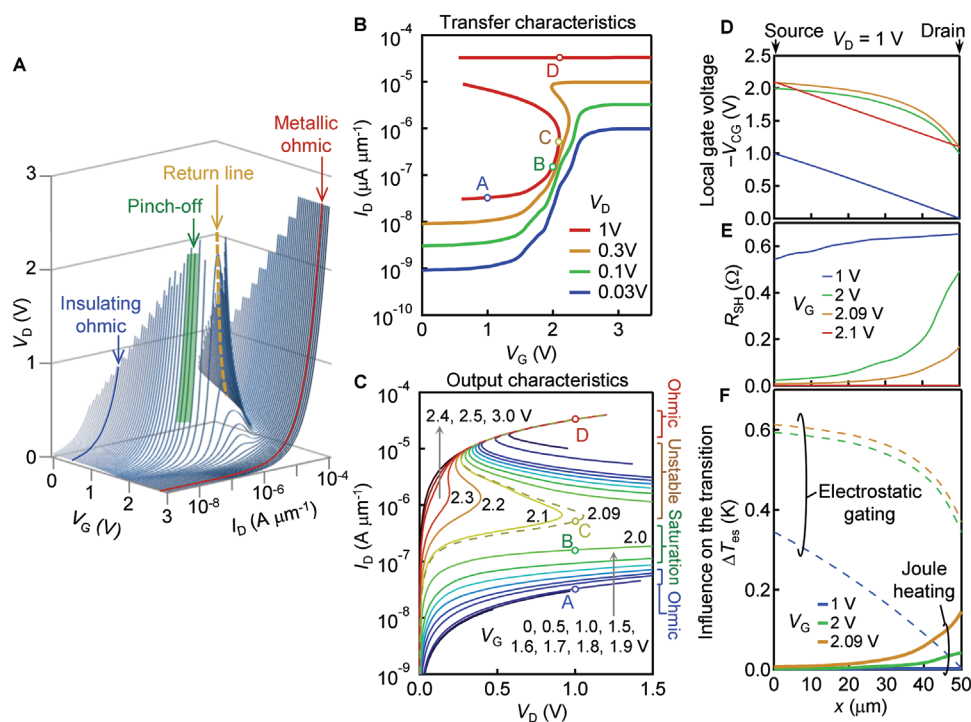


Figure 5. Device simulation. A) Simulated V_G , V_D , and I_D values at the steady state of the VO_2 -channel three-terminal device. B) Simulated transfer characteristics that correspond to the cross sections of (A) at four different V_D values. C) Simulated output characteristics that correspond to the cross sections of (A) at various V_G values. D,E) Local gate voltage ($-V_{GG}$) and the sheet resistance (R_{SH}) in the VO_2 channel as a function of the distance from the source (x) for $V_D = 1$ V and four different V_G values. F) Comparison of the electrostatic gating effect and the Joule heating effect at each position inside the VO_2 channel. The comparison is made by the increase in the local electrostatic temperature (ΔT_{es}).

Interestingly, the negative differential resistance region is observed in Figure 5A, which is due to the fact that the resistance of the phase transition material decreases at a rapid rate that exceeds the increase rate of current. While such negative differential resistance is commonly reported in the VO_2 two-terminal devices,^[29,30] Figure 5A extends the concept to the three-terminal device, showing the negative conductance for I_D versus V_D and the negative transconductance for I_D versus V_G . The negative differential resistance region is also related to the instability of the phase transition under the constant voltage (Figure S3, Supporting Information), and leads to a discontinuous jump that is observed in the voltage sweep measurement (Figures 2A and 3).

It is worth noting that in spite of the non-negligible Joule heating at the drain, the metallic transition always proceeds from the source until the discontinuous jump takes place. This is clearly observed by the sum of the electrostatic gating effect and the Joule heating effect (Figure 5F) that is always larger at the source than at the drain, irrespective of the V_G value. Even for the value of $V_G = 2.09$ V at which the Joule heating is almost maximized, the sum of ΔT_{es} at the source is 0.62 K, and is larger than 0.56 K at the drain. Indeed, the Joule heating takes place in the most insulating region in the channel, in other words, in the region with the minimum ΔT_{es} . Thus, the Joule heat only compensates the locally small ΔT_{es} and has little effect of driving the transition. Conversely, the local gate voltage is always stronger by V_D at the source than at the drain, and drives the transition from the source. In this sense, even

at large V_D , the electrostatic gating is primarily responsible for the transition, and the V_D -induced Joule heating is regarded as the secondary effect. It should be noted that the thermal effect is still essential for the abruptness as shown below and also in Figure S3, Supporting Information.

In order to clearly understand the pinch-off effect and the V_D effect, we simulated the transfer characteristics of I_D versus V_G when either the electrostatic gating effect or the Joule heating effect is ignored intentionally. In the case that the electrostatic gating alone is considered (Figure 6A), the characteristics at small V_D are the same as those in Figure 5B, and a pinch-off effect is also observed near the transition point, where the I_D

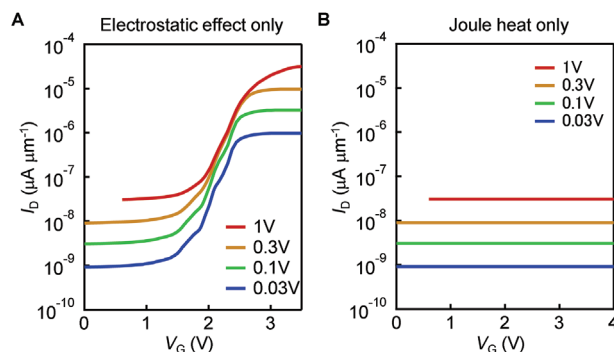


Figure 6. Electrostatic effect versus Joule heating effect. A) Simulated transfer characteristics with electrostatic gating effect alone. B) Simulated transfer characteristics with Joule heating effect alone.

becomes independent of V_D . However, the transition does not become steeper because of the absence of the Joule heating. On the other hand, if the electrostatic effect is ignored (Figure 6B), the V_G no longer matters and the transition does not occur. In other words, the experimentally observed steepening of the transition can only be reproduced by mainly the electrostatic gating and the extra catalytic effect of Joule heating. A detailed explanation of the catalytic effect of Joule heat is given in Supporting Information.

3. Conclusion

In conclusion, we successfully induce a complete metal-insulator transition throughout the VO_2 channel by solid-state electrostatic gating. This solid-state gating enables a systematic study of this new class of three-terminal devices, and the pinch-off effect is observed for the first time in phase transition devices, corroborating the electrostatic effects underlying the device operation. In addition, the application of the large V_D results in a strong “catalytic” effect of steepening the transition, leading to the gate-induced transition even by the application of 0.1 V gate voltage. Both of these three-terminal properties are reproduced in quasi-equilibrium models, and could be the basis for a variety of electronic devices that utilize phase transitions, such as ferroelectric negative capacitance^[31] and materials-based neuromorphic devices.^[32,33] Furthermore, this three-terminal geometry can be used in materials science research as well, enabling high-speed and high-resolution control of material phases in the vicinity of the transition point, and revealing transient properties that have been unclear so far.

4. Experimental Section

VO₂-Channel Three-Terminal Device: The 7 nm VO_2 thin film was epitaxially grown on the Nb 0.05 wt% doped TiO_2 (101) substrate at the substrate temperature of 325 °C, an O_2 pressure of 2 Pa, and a laser energy density of 0.5 J cm⁻² with an excimer laser with a wavelength of 248 nm. The lithography photoresist masks with 50 μm widths (corresponding to the VO_2 channel length) were patterned on the VO_2 surface. In turn, Au was evaporated and lifted off to form the bare VO_2 region. The photoresist masks were further patterned on the top to define the area of the device, including the source, the drain, and the channel. With the use of the masks, Au and VO_2 were etched by the Au etchant and the 0.79 wt% NaIO_4 solution, respectively. The Au pads (source and drain) were manually bonded to the Al wire with Ag paste, and the Nb-doped TiO_2 substrate was ultrasonically bonded with Al wire as the gate contact. All the electrical properties of the inverse Schottky gate are summarized elsewhere.^[18]

Measurements: The transfer and the output characteristics were measured with a semiconductor parameter analyzer (B1500, Keysight Technologies), and the resistance data were measured with a general-purpose digital source meter (2400, Keithley Instruments). In Figure 2A, I_D yielded small steps that reflect the discrete domain structure. I_D did not recover to its initial value when V_G was reset to zero because the electrostatic control was weaker than the transition hysteresis. The lack of data at $V_G < V_D$ was because the authors avoided the large negative gate leakage current owing to the forward biased Schottky junction at the drain-gate interface.

Definition of Electrostatic Temperature: For the small V_D , the VO_2 channel could be regarded as a homogeneous resistor, and its resistance was simply determined by the temperature and

the V_G . The V_G accumulated electrons in the VO_2 channel with the areal density proportional to $(V_G + V_b)^{1/2} - V_b^{1/2}$ in the inverse Schottky gate,^[23] and decreased the transition temperature (T_{MIT}) by $a\{(V_G + V_b)^{1/2} - V_b^{1/2}\}$.^[18] The linear coefficient $a = 0.73 \text{ KV}^{-1/2}$ was extracted from Figure 4B. The Joule heating effect in the small- V_D condition was ignored, and then, the transition of the VO_2 channel was simply induced by $T_0 + \Delta T + a\{(V_G + V_b)^{1/2} - V_b^{1/2}\}$, where T_0 was the reference temperature (323.5 K for example), and ΔT was the temperature variation from T_0 in the measurement system. The last term was attributed to the increased accumulated carrier density by V_G . Therefore, if one defined the electrostatic temperature T_{es} by $T_{\text{es}} = T_0 + \Delta T + a\{(V_G + V_b)^{1/2} - V_b^{1/2}\}$, the influence of the V_G could be incorporated as shown in Figure 4D.

Simulations: In order to discuss the large- V_D case, the Joule heating effect had to be considered. Along with the local electrostatic effect from the gate, the local Joule heating effect modulated the VO_2 local sheet resistance $R_{\text{SH}}(x)$. Because the VO_2 channel was relatively large (several tens μm), one could average the microscopic domain structure and assume a smooth function of the VO_2 local sheet resistance $R_{\text{SH}}(x)$. It was assumed that the $R_{\text{SH}}(x)$ could be determined by the local electrostatic temperature $T_{\text{es}}(x)$, and the Joule heating effect could be incorporated in the ΔT term of the above T_{es} equation. This time, the T_0 was the measurement temperature (323.5 K), and the ΔT was the Joule heating effect which equaled $I_D^2 R_{\text{SH}}(x)/D$, where I_D was the sheet current, and D was the effective thermal conductance to the surroundings.^[34] The variable D was the fitting parameter that was set to $3 \times 10^5 \text{ WK}^{-1} \text{ m}^{-2}$ in this simulation. If the thermal conductivity of the Nb:TiO₂ substrate was assumed to be of the order of $10 \text{ Wm}^{-1}\text{K}^{-1}$,^[35] this D value indicated that the thermal gradient was formed inside the substrate within a distance of 30 μm from the interface. This distance was physically reasonable in a sense that it was in the same order as the channel width 50 μm and the channel length 35 μm, respectively. The local electrostatic temperature was $T_{\text{es}}(x) = T_0 + I_D^2 R_{\text{SH}}(x)/D + a\{(-V_{\text{CG}}(x) + V_b)^{1/2} - V_b^{1/2}\}$, where $-V_{\text{CG}}(x)$ was the local gate voltage, $-V_{\text{CG}}(0) = V_G$, and $-V_{\text{CG}}(L) = V_G - V_D$. This $T_{\text{es}}(x)$ value determined $R_{\text{SH}}(x)$ by $R_{\text{SH}}(x) = f(T_{\text{es}})$, where the function $f()$ was the temperature dependence of the VO_2 sheet resistance in the two-terminal geometry, and experimentally obtained from Figure 4D. The expression of $V_{\text{CG}}(x)$ followed the local Ohm's law: $dV_{\text{CG}}(x)/dx = I_D R_{\text{SH}}(x)$. By combining these two equations with the boundary condition $-V_{\text{CG}}(0) = V_G$, $V_{\text{CG}}(x)$ and the $R_{\text{SH}}(x)$ could be calculated for fixed I_D and V_G values. Accordingly, V_D was obtained by $V_{\text{CG}}(L) = -(V_G - V_D)$. By iterating this calculation for various I_D and V_G values, the 3D map of the steady state in Figure 5A was obtained. In Figure 5F, the influences of the accumulated electrons $a\{(-V_{\text{CG}}(x) + V_b)^{1/2} - V_b^{1/2}\}$ and the Joule heating $I_D^2 R_{\text{SH}}(x)/D$ were plotted as functions of x , respectively.

Supporting Information

Supporting Information is available from the Wiley Online Library or from the author.

Acknowledgements

The authors thank Dr. Isao Inoue in The National Institute of Advanced Industrial Science and Technology, Japan, Dr. Yusuke Kozuka in National Institute of Materials Science, Japan, and Prof. Ken Uchida and Prof. Takahisa Tanaka in The University of Tokyo, Japan for the scientific discussion. This research was supported by JSPS KAKENHI 20H02615, and was partially supported by JSPS KAKENHI 18H03686.

Conflict of Interest

The authors declare no conflict of interest.

Data Availability Statement

The data that support the findings of this study are available from the corresponding author upon reasonable request.

Keywords

electrostatic gating, metal-insulator transition, Mott transistor, Schottky junction, vanadium oxide

Received: August 11, 2021

Revised: October 11, 2021

Published online: November 21, 2021

- [1] J. Chakhalian, J. W. Freeland, A. J. Mills, C. Panagopoulos, J. M. Rondinelli, *Rev. Mod. Phys.* **2014**, *86*, 1189.
- [2] C. H. Ahn, J.-M. Triscone, J. Mannhart, *Nature* **2003**, *424*, 1015.
- [3] P. Baum, D.-S. Yang, A. H. Zewail, *Science* **2007**, *318*, 788.
- [4] V. R. Morrison, R. P. Chatelain, K. L. Tiwari, A. Hendaoui, A. Bruhács, M. Chaker, B. J. Siwick, *Science* **2014**, *346*, 445.
- [5] D. Lee, B. Chung, Y. Shi, G.-Y. Kim, N. Campbell, F. Xue, K. Song, S.-Y. Choi, J. P. Podkaminer, T. H. Kim, P. J. Ryan, J.-W. Kim, T. R. Paudel, J.-H. Kang, J. W. Spinuzzi, D. A. Tenne, E. Y. Tsybal, M. S. Rzechowski, L. Q. Chen, J. Lee, C. B. Eom, *Science* **2018**, *362*, 1037.
- [6] Z. Yang, Y. Zhou, S. Ramanathan, *J. Appl. Phys.* **2012**, *111*, 014506.
- [7] M. Nakano, K. Shibuya, D. Okuyama, T. Hatano, S. Ono, M. Kawasaki, Y. Iwasa, Y. Tokura, *Nature* **2012**, *487*, 459.
- [8] Y. Zhou, S. Ramanathan, *J. Appl. Phys.* **2012**, *111*, 084508.
- [9] H. Ji, J. Wei, D. Natelson, *Nano Lett.* **2012**, *12*, 2988.
- [10] K. Liu, D. Fu, J. Cao, J. Suh, K. X. Wang, C. Cheng, D. F. Ogletree, H. Guo, S. Sengupta, A. Khan, C. W. Yeung, S. Salahddin, M. M. Deshmukh, J. Wu, *Nano Lett.* **2012**, *12*, 6272.
- [11] J. S. Sim, Y. Zhou, S. Ramanathan, *Nanoscale* **2012**, *4*, 7056.
- [12] J. Jeong, N. Aetukuri, T. Graf, T. D. Schladt, M. G. Samant, S. S. P. Parkin, *Science* **2013**, *339*, 1402.
- [13] G. Stefanovich, A. Pergament, D. Stefanovich, *J. Phys.: Condens. Matter* **2000**, *12*, 8837.
- [14] H.-T. Kim, B.-G. Chae, D.-H. Youn, S.-L. Maeng, G. Kim, K.-Y. Kang, Y.-S. Lim, *New J. Phys.* **2004**, *6*, 52.
- [15] D. Ruzmetov, G. Gopalakrishnan, C. Ko, V. Narayanamurti, S. Ramanathan, *J. Appl. Phys.* **2010**, *107*, 114516.
- [16] S. Sengupta, K. Wang, K. Liu, A. K. Bhat, S. Dhara, J. Wu, M. M. Deshmukh, *Appl. Phys. Lett.* **2011**, *99*, 062114.
- [17] M. M. Qazilbash, Z. Q. Li, P. M. Brehm, F. Keilmann, B. G. Chae, H. T. Kim, D. N. Basov, *Appl. Phys. Lett.* **2008**, *92*, 241906.
- [18] T. Yajima, T. Nishimura, A. Toriumi, *Nat. Commun.* **2015**, *6*, 10104.
- [19] F. J. Morin, *Phys. Rev. Lett.* **1959**, *3*, 34.
- [20] J. H. Park, J. M. Coy, T. S. Kasirga, C. Huang, Z. Fei, S. Hunter, D. H. Cobden, *Nature* **2013**, *500*, 431.
- [21] J. B. Goodenough, *J. Solid State Chem.* **1971**, *3*, 490.
- [22] K. Shibuya, M. Kawasaki, Y. Tokura, *Appl. Phys. Lett.* **2010**, *96*, 022102.
- [23] S. M. Sze, K. K. Ng, *Physics of Semiconductor Devices*, 3rd ed., John Wiley & Sons, Hoboken, NJ, USA **2007**.
- [24] M. M. Qazilbash, M. Brehm, B.-G. Chae, P.-C. Ho, G. O. Andreev, B.-J. Kim, S. J. Yun, A. V. Balatsky, M. B. Maple, F. Keilmann, H.-T. Kim, D. N. Basov, *Science* **2007**, *318*, 1750.
- [25] T. Yajima, Y. Ninomiya, T. Nishimura, A. Toriumi, *Phys. Rev. B* **2015**, *91*, 205102.
- [26] J. Wu, Q. Gu, B. S. Guiton, N. P. De Leon, L. Ouyang, H. Park, *Nano Lett.* **2006**, *6*, 2313.
- [27] T. Yajima, T. Nishimura, A. Toriumi, *Small* **2017**, *13*, 1603113.
- [28] A. Zimmers, L. Aigouy, M. Mortier, A. Sharoni, S. Wang, K. G. West, J. G. Ramirez, I. K. Schuller, *Phys. Rev. Lett.* **2013**, *110*, 056601.
- [29] W. Löser, C. Mattheck, W. Haubenreisser, *Phys. Status Solidi A* **1974**, *21*, 487.
- [30] T. Yajima, T. Nishimura, A. Toriumi, in *2016 IEEE Int. Electron Devices Meeting*, IEEE, Manhattan, NY, USA **2016**, p. 853.
- [31] M. Hoffmann, F. P. G. Fengler, M. Herzig, T. Mittmann, B. Max, U. Schroeder, R. Negrea, P. Lucian, S. Slesazeck, T. Mikolajick, *Nature* **2019**, *565*, 464.
- [32] M. D. Pickett, G. Medeiros-Ribeiro, R. S. Williams, *Nat. Mater.* **2013**, *12*, 114.
- [33] W. Yi, K. K. Tsang, S. K. Lam, X. Bai, J. A. Crowell, E. A. Flores, *Nat. Commun.* **2018**, *9*, 4661.
- [34] J. S. Brockman, L. Gao, B. Hughes, C. T. Rettner, M. G. Samant, K. P. Roche, S. S. P. Parkin, *Nat. Nanotechnol.* **2014**, *9*, 453.
- [35] W. R. Thurber, A. J. H. Mante, *Phys. Rev. A* **1965**, *139*, A1655.